Socioeconomic Drivers of Post-Rainstorm Community Resilience: A comparative analysis of two cases in North China

Qi Wang
Tsinghua University, School of Safety Science
wangq_0610@163.com

Feihu Sun
Tsinghua University, Hefei Institute of Public Safety Research
fhsun98@163.com

Tao Chen
Tsinghua University, School of Safety Science
chentao.b@tsinghua.edu.cn

Guofeng Su
Tsinghua University, School of Safety Science
sugf@tsinghua.edu.cn

Lida Huang
Tsinghua University, School of Safety Science
huanglida@mail.tsinghua.edu.cn

ABSTRACT

Short-duration and high-intensity extreme rainfall events increasingly disrupt urban systems. Under escalating climate risks, understanding post-disaster recovery dynamics has become critical for resilience assessment and recovery planning. However, research on post-rainstorm recovery remains constrained by limited data availability, insufficient temporal resolution, and inadequate identification of spatiotemporal heterogeneity in recovery trajectories. To address these limitations, this study uses daily NASA VIIRS nighttime light (NTL) time-series data as a proxy for observable functional recovery in two flood-affected areas in North China following the July–August 2023 extreme rainfall event. A pixel-level Recovery Rate Index is constructed to quantify rebound dynamics, and time-series clustering is applied to identify distinct recovery trajectories. Explanatory modeling is further conducted to examine the socioeconomic and environmental drivers associated with different recovery modes. Results show that recovery regimes differ substantially across terrain contexts. The comparison further suggests that mountainous and plain urban environments are characterized by different dominant recovery mechanisms, highlighting the need for geographically differentiated post-disaster recovery assessment and resilience planning.

Keywords

Extreme rainfall, nighttime lights, disaster recovery, community resilience.

INTRODUCTION

Extreme rainfall events have become increasingly frequent and intense under the combined influence of climate change and rapid urbanization, generating substantial disruptions to urban infrastructure systems and community life. Urban flood disasters not only damage physical assets but also interrupt electricity supply, transportation services, commercial activities, and essential public services, thereby affecting the daily functioning of communities (IPCC, 2023). Within the disaster risk management framework, resilience is increasingly understood not merely as the capacity to resist or absorb shocks, but also as the ability of a system to restore functionality after disturbance (Lopes et al., 2025; Rose & Dormady, 2018). In this context, post-disaster recovery has emerged

as a critical empirical dimension for evaluating urban and community resilience.

Recent research reflects a clear shift from static assessments of exposure and vulnerability toward dynamic analyses of recovery trajectories. Early resilience studies largely relied on indicator-based composite indices constructed from socioeconomic and infrastructural variables (Cutter, 2016). While valuable for comparative assessment, such approaches are typically cross-sectional and insufficient to capture the temporal evolution of system functionality after disaster. Recent studies increasingly focus on recovery pathways, which capture time-dependent changes in infrastructure operation, accessibility, economic activity, and population presence and are widely considered observable expressions of systemic resilience (Yabe et al., 2020; Jiang et al., 2023; Rose & Dormady, 2018).

However, quantitative characterization of recovery dynamics faces significant data constraints. Traditional assessments commonly depend on household surveys, administrative statistics, or official damage reports. Although these sources provide important contextual information, they often suffer from coarse spatial resolution, limited temporal frequency, and reporting delays (Cutter, 2016). Such limitations hinder fine-scale, time-sensitive analysis of short-term disturbance and recovery phases, especially in rapidly evolving post-disaster contexts. To address these challenges, an expanding body of literature has turned to satellite-derived nighttime light (NTL) data to monitor disaster impacts and recovery processes. Nighttime light intensity has been widely used as a proxy for economic activity, infrastructure functionality, and human presence (Zheng et al., 2023). Studies using DMSP/OLS, VIIRS Black Marble, and SDGSAT-1 datasets demonstrate that abrupt declines in NTL brightness can effectively capture electricity outages and functional disruptions following disasters, while gradual restoration of brightness reflects the resumption of socioeconomic activities (Wang et al., 2018; Qiang et al., 2020; Zhang et al., 2023; Tang & Zhang, 2025). Moreover, time-series analysis of NTL data enables the identification of disturbance magnitude, recovery duration, and rebound speed, providing an intuitive and temporally continuous indicator of post-disaster system performance. At the same time, NTL should not be interpreted as a complete measure of community resilience. Rather, it more directly captures visible functional restoration associated with electricity-dependent activity, built-up area functioning, and nighttime socioeconomic resumption, while other dimensions such as health services, food provision, telecommunications, and social support may remain only partially observed.

Importantly, recovery processes are not spatially uniform. Evidence from mobility and activity-based datasets indicates that post-disaster rebound often exhibits significant spatial inequality, with communities characterized by differing socioeconomic conditions experiencing divergent recovery speeds and trajectories (Yabe et al., 2020; Jiang et al., 2023). Similarly, recent studies integrating NTL data with socioeconomic indicators reveal that pre-existing economic structures, population density, and infrastructure capacity shape the pace and pattern of post-disaster restoration (Tang & Zhang, 2025; Shu et al., 2025). These findings highlight the necessity of linking observable recovery dynamics with underlying socioeconomic drivers.

Despite these advances, two limitations remain prominent in existing research. First, many NTL-based recovery studies rely on monthly composites or simple pre- and post-event comparisons (Li et al., 2018; Qiang et al., 2020), limiting their ability to capture short-term fluctuations and intra-event variability following extreme rainfall. Second, although heterogeneous recovery patterns have been documented, systematic comparative analysis of community-level recovery trajectories and their socioeconomic determinants remains relatively underdeveloped.

To address these gaps, this study investigates post-rainstorm recovery heterogeneity through a comparative analysis of two flood-affected areas in North China. By integrating daily nighttime light time-series data with community-level socioeconomic and environmental indicators, we quantify pixel-level recovery trajectories and examine their spatial divergence across contrasting terrain contexts. This study makes three contributions. First, it extends daily NTL-based recovery analysis to post-rainstorm recovery, a context that remains less systematically examined than earthquakes, blackouts, or other infrastructure-disruptive hazards. Second, by comparing a mountainous suburban district and a plain urban area affected by the same extreme rainfall event, it develops a cross-case perspective on how terrain context conditions recovery heterogeneity. Third, it interprets recovery differentiation through two broader mechanisms, terrain-mediated and economically-mediated recovery, thereby linking observable recovery trajectories to context-specific resilience processes. Rather than treating NTL as a complete representation of community resilience, this study uses it as a scalable empirical lens on visible functional recovery and its socioeconomic differentiation.

METHOD

Study Design and Case Context

This study adopts a comparative design to examine heterogeneous post-rainstorm recovery processes across two

flood-affected areas in North China: Mentougou District (Beijing) and Zhuozhou City (Hebei Province). The two cases were impacted by the same extreme rainfall event in late July–August 2023, yet differ markedly in terrain conditions and settlement patterns. Mentougou is predominantly mountainous with constrained accessibility, where damaged lifeline infrastructure and disrupted services may exhibit prolonged recovery. Zhuozhou is located on the North China Plain with extensive built-up areas and widespread inundation, providing a contrasting recovery context.

An integrated analytical workflow was implemented to ensure methodological consistency across cases: (1) derive pixel-level recovery indicators from daily VIIRS nighttime lights; (2) identify representative recovery trajectories using time-series clustering; and (3) quantify the association between recovery heterogeneity and socioeconomic–environmental drivers using statistical tests and explanatory models (Figure 1). Because the objective of this study is to compare recovery differentiation across terrain contexts under a common disaster event, all analytical steps were implemented using a harmonized spatial framework. Both case studies were aligned to the same VIIRS-based 500 m grid and analyzed using the same sequence of recovery metric construction, trajectory classification, and explanatory modeling. This design ensures comparability while preserving case-specific heterogeneity in the interpretation of recovery dynamics.

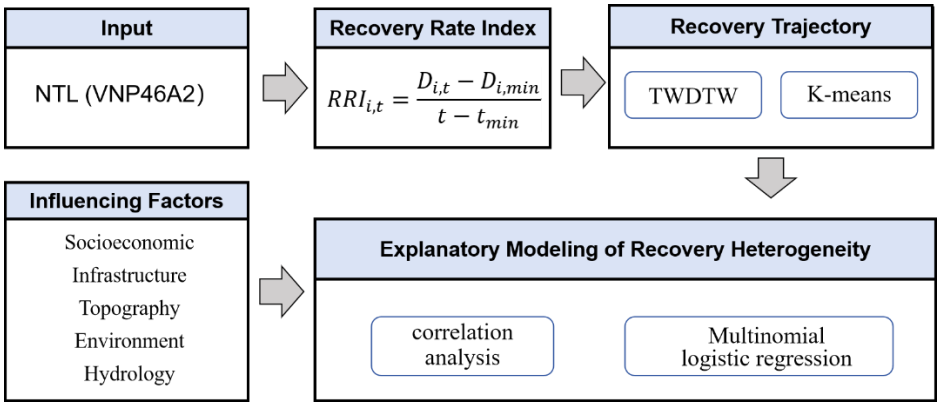

Figure 1. Research framework

Nighttime Light Data and Recovery Rate Index

Daily nighttime light (NTL) observations were obtained from the NASA Black Marble VIIRS VNP46A2 product at 500 m spatial resolution. The dataset includes corrections for lunar illumination, BRDF effects, and atmospheric conditions, enabling temporally consistent radiance comparisons (Román et al., 2018). The analysis period covers the disaster impact and subsequent recovery stage, from 29 July to 31 August 2023. All datasets were reprojected to WGS 1984 UTM Zone 50N and resampled to 500 m to match the VIIRS grid.

To quantify pixel-level recovery dynamics, we computed a Recovery Rate Index (RRI) that captures the average rebound rate of nighttime light brightness following disaster-induced disruption. For each pixel i and day t, RRI is defined as:

$$RRI_{i,t} = \frac{D_{i,t} - D_{i,min}}{t - t_{min}}$$

Where $D_{i,t}$ is the NTL brightness at time t, $D_{i,min}$ is the minimum brightness observed after the disaster, t_{min} is the day when this minimum occurs. The numerator represents brightness rebound from the post-disaster trough, while the denominator is the elapsed time since the trough, yielding an average recovery slope. Pixels with persistent outage or negligible rebound have RRI values near zero, whereas areas with rapid restoration show higher positive values. Compared with using absolute post-disaster brightness alone, RRI emphasizes the rate and timing of rebound after the disruption trough and is therefore better suited to distinguishing heterogeneous recovery trajectories. In this study, the metric is interpreted as an indicator of observable post-disaster rebound rather than a complete measure of resilience.

To ensure temporal stability and reduce noise from missing observations, RRI was computed only for pixels with at least five valid post-disaster NTL observations. Prior to analysis, brightness values were normalized to minimize the influence of absolute luminosity differences across land uses, so that the subsequent clustering and modeling focus on recovery dynamics rather than baseline brightness.

Recovery Trajectory Classification

To characterize heterogeneous recovery dynamics, clustering was applied to the daily RRI time series for all valid pixels. Temporal similarity between pixel-level trajectories was measured using Time-Weighted Dynamic Time Warping (TWDTW), which extends classical DTW by introducing time-penalty weights. This allows trajectories with similar recovery shapes but shifted timing to be matched while penalizing unrealistic temporal misalignment, which is particularly suitable for post-disaster recovery processes that may start at different times across space.

Pairwise TWDTW distances were computed to form a distance matrix, which was then used for clustering to identify distinct recovery modes. Internal validity criteria, including the Silhouette Coefficient and Elbow Method, were first examined within each case to identify interpretable candidate solutions. Because both cases showed reasonable separation around K = 5 and because direct cross-case comparison was a core objective of the study, the final analysis adopted five recovery clusters for both Mentougou and Zhuozhou. The clustered raster was subsequently post-processed with a 3×3 majority filter to reduce salt-and-pepper noise and improve spatial coherence. For each recovery mode, we summarized its median trajectory and dispersion (e.g., interquartile range) and mapped its spatial distribution to support cross-case comparison.

Explanatory Modeling of Recovery Heterogeneity

To investigate the drivers of recovery heterogeneity, we assembled a parsimonious set of socioeconomic, infrastructure, topographic, environmental, and hydrological variables that jointly capture economic capacity, settlement intensity, accessibility, and physical constraints on post-disaster recovery. Eight variables were selected based on both theoretical relevance and cross-case data comparability: GDP density, population density, settlement density, road density, elevation, slope, NDVI, and distance to river (Table 1). These variables do not aim to exhaustively represent all dimensions of community resilience; rather, they provide a spatially comparable set of indicators for examining how recovery differentiation is associated with pre-existing structural conditions in the two study areas.

Table 1. Description of potential factors influencing recovery trajectory

Category	Variable	Description
Socioeconomic	GDP density (yuan/km²)	Economic activity and capital availability
	Population density (persons/km²)	Labor availability and exposure
	Settlement density	Compactness of built-up areas
Infrastructure	Road density (km/km²)	Accessibility for emergency and repair operations
Topography	Elevation (m)	Terrain constraints, exposure, difficulty of repair
	Slope (°)	Construction feasibility, hazard susceptibility
Environment	NDVI (%)	Vegetation cover and ecological buffering
Hydrology	Distance to river (m)	Exposure to flooding and accessibility

All explanatory datasets were aligned to the VIIRS grid using a common projection and 500 m spatial resolution. Continuous variables were standardized using Z-score normalization prior to statistical analysis in order to make coefficient magnitudes comparable across predictors. GDP density and population density were used to represent economic capacity and human concentration. Settlement density reflects the compactness of built-up areas, while road density captures accessibility relevant to emergency access and repair operations. Elevation and slope represent terrain-related constraints, NDVI reflects land-cover and ecological context, and distance to river captures hydrological exposure and proximity to flood-prone corridors.

We first used Spearman's rank correlation to assess monotonic associations between recovery indicators and explanatory variables. Three recovery indicators were included: (1) Mean RRI (overall recovery rate), (2)

Maximum RRI (peak recovery intensity), (3) Recovery start time (delay before recovery onset). This analysis captures general trends and potential nonlinear relationships without requiring parametric assumptions.

Next, Kruskal–Wallis tests were conducted to determine whether different recovery trajectory groups were associated with significantly different structural conditions. Given the non-normality and spatial heterogeneity of several predictors, this non-parametric approach was used to compare groupwise differences across the eight explanatory variables, with epsilon-squared reported as an indicator of effect size.

Finally, separate multinomial logistic regression models were estimated for Mentougou and Zhuozhou to evaluate the combined effects of multiple predictors on recovery trajectory membership. The dependent variable was the pixel-level recovery trajectory class, and the explanatory variables were the eight standardized structural factors. By incorporating all predictors simultaneously, the model enables identification of the dominant factors associated with different recovery trajectories while accounting for inter-variable dependence. Coefficients were interpreted in terms of the direction and relative magnitude of association between each predictor and trajectory assignment. Case-specific estimation further preserves contextual heterogeneity and facilitates cross-case comparison of recovery mechanisms.

RESULTS

Post-Rainstorm Recovery in Mentougou District

Daily NTL-derived recovery indices reveal pronounced spatiotemporal heterogeneity in Mentougou District following the July 2023 extreme rainfall event. Time-series clustering of pixel-level RRI trajectories identified five distinct recovery patterns, primarily differentiated by recovery onset timing and intensity. The optimal cluster number (K=5) was supported by multiple internal validity metrics (Silhouette=0.203; Calinski–Harabasz=32.48; Davies–Bouldin=1.84), indicating satisfactory separation between recovery modes.

The five clusters account for 18.1%, 27.0%, 17.3%, 12.3%, and 25.3% of valid pixels, respectively, demonstrating substantial heterogeneity even within a single mountainous suburban district (Figure 2).

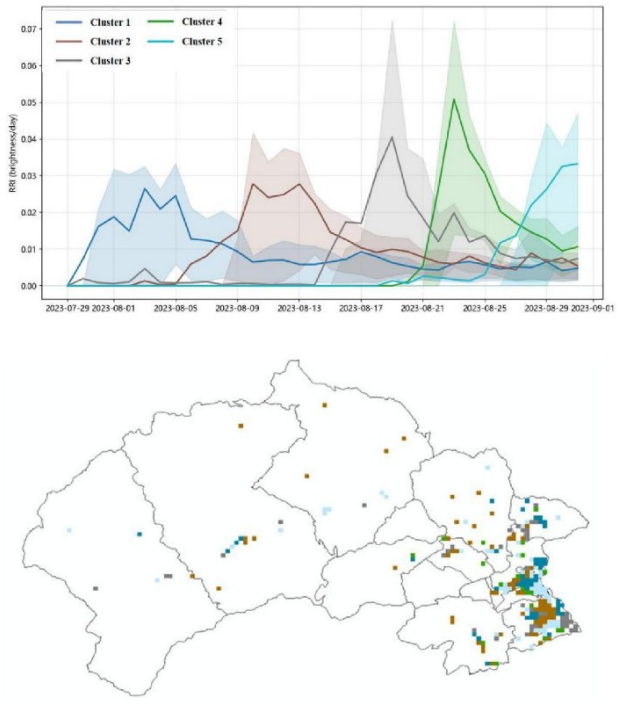

Figure 2. Median recovery trajectories and spatial distribution of the five recovery clusters in Mentougou District

Cluster 1 (18.1%) represents early-onset rapid recovery. Pixels in this group exhibited a sharp rise in RRI immediately after the post-disaster trough, sustaining high recovery rates for approximately 7–10 days before tapering. Spatially, these areas concentrate along major transportation corridors and high-priority functional zones, suggesting early restoration of critical infrastructure.

Cluster 2 (27.0%) displays a delayed but sustained recovery trajectory. Recovery remained near zero during the first week and gradually increased in early-to-mid August, forming a stable medium-level plateau. These areas correspond largely to residential neighborhoods and secondary road networks where repair activities commenced after emergency zones were secured.

Cluster 3 (17.3%) is characterized by mid-term pulse recovery. After minimal early activity, a short-lived but high-intensity recovery peak emerged around mid-August, likely reflecting concentrated repair interventions following preliminary assessments.

Cluster 4 (12.3%) represents late but fast recovery, with negligible RRI values until late August, followed by a rapid spike. This pattern is consistent with locations dependent on upstream lifeline restoration, where recovery could only begin once key network segments were reconnected.

Cluster 5 (25.3%) exhibits very late or ongoing recovery, with RRI values remaining near zero for most of the observation period. Some pixels continued rising toward the end of August, indicating prolonged disruption or incomplete restoration one month after the event. These areas likely correspond to structurally constrained or topographically isolated zones.

Spatially, recovery activity was concentrated in the southeastern built-up valley areas and along the main river corridor, while high-elevation western mountainous regions exhibited sparse detectable recovery signals. This uneven spatial distribution reflects the combined effects of settlement density, accessibility, and baseline luminosity constraints inherent to mountainous environments.

Correlation analysis further indicates that mean and maximum RRI values are positively associated with population density ($\rho \approx 0.48$), settlement density ($\rho \approx 0.46$), and GDP density ($\rho \approx 0.37$), suggesting that areas with stronger socioeconomic intensity experienced faster and stronger recovery. In contrast, elevation shows a negative association ($\rho \approx -0.28$), indicating delayed recovery at higher altitudes where terrain constraints limit accessibility. Other environmental variables, including slope, NDVI, and distance to river, display comparatively weak monotonic relationships (Figure 3).

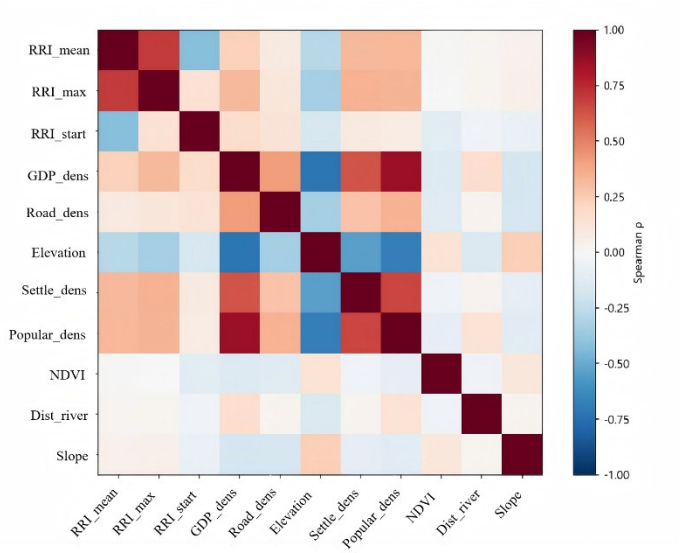

Figure 3. Spearman correlation analysis in Mentougou District

Kruskal–Wallis tests confirm statistically significant groupwise differences across recovery types. Population density ($H=9.40$, $p=0.0517$) and distance to river ($H= 8.58$, $p= 0.0724$) exhibit the strongest divergence among clusters, albeit with modest effect sizes ($\varepsilon^2 \approx 0.02$). GDP density also demonstrates moderate variation ($H=7.61$). In contrast, elevation and road density show weaker standalone group differentiation.

Multinomial logistic regression reveals distinct combinations of drivers across recovery modes (Table 2). Population density consistently increases the likelihood of belonging to early-onset recovery clusters ($\beta \approx +0.46$), while elevation and slope contribute to delayed or prolonged recovery trajectories. Road density is positively associated with mid-term pulse recovery ($\beta \approx +0.35$), highlighting the importance of network connectivity for concentrated repair activities. GDP density emerges as a positive predictor for very late or ongoing recovery ($\beta \approx +0.36$), suggesting that economically significant but topographically constrained areas may experience extended disruption.

Taken together, the Mentougou case demonstrates that post-disaster recovery in mountainous suburban districts is shaped by a complex interplay between functional priority, network connectivity, and terrain-imposed accessibility constraints. Socioeconomic intensity facilitates early rebound, whereas elevation and slope contribute to delayed restoration trajectories.

Table 2. Impact factors of each recovery cluster in Mentougou

Cluster	Proportion	Main positive factors	Main negative factor
C1	18.1%	Population density (+0.46), Distance to river (+0.25)	Slope (-0.23)
C2	27.0%	Elevation (+0.26), Settlement density (+0.38), Slope (+0.23)	Population density (-0.24)
C3	17.3%	Road density (+0.35), NDVI (+0.10)	Elevation (-0.43), Population density (-0.30), Settlement density (-0.41)
C4	12.3%	Settlement density (+0.14), Distance to river (+0.13)	Road density (-0.09)
C5	25.3%	GDP density (+0.36), Elevation (+0.27), Slope (+0.15)	NDVI (-0.13), Distance to river (-0.15)

Post-Rainstorm Recovery in Zhuozhou City

In contrast to the mountainous recovery structure observed in Mentougou, daily NTL-derived recovery indices in Zhuozhou reveal a more evenly distributed yet temporally stratified recovery process following the July 2023 extreme rainfall event. Time-series clustering of pixel-level RRI trajectories likewise identified five distinct recovery patterns, differentiated primarily by recovery onset timing and rebound intensity. To ensure methodological consistency across cases and facilitate direct comparison, the cluster number was fixed at K=5.

The five clusters account for 20.05%, 24.67%, 18.07%, 16.89%, and 20.32% of valid pixels, respectively, indicating a relatively even distribution across recovery modes without a single dominant trajectory (Figure 4).

Cluster 1 (20.05%) represents early but moderate recovery. Pixels in this group show a rapid rebound shortly after the post-disaster trough, followed by gradual stabilization. These areas are moderately associated with higher GDP (β=0.2341) and elevation (β=0.2253), while negatively associated with population density (β=-0.1904), suggesting relatively elevated but less densely populated zones where restoration proceeded steadily.

Cluster 2 (24.67%), the largest group, exhibits early and sustained recovery. Recovery rates increase gradually and remain stable throughout mid-August. This cluster shows positive associations with GDP (β=0.2444) and distance to river (β=0.1489), indicating that economically stronger and relatively river-distant areas were more likely to experience sustained rebound.

Cluster 3 (18.07%) displays a mid-term pulse recovery pattern characterized by delayed onset followed by a short-lived increase. Although coefficients remain moderate, road density (β=0.1133) and NDVI (β=0.0835) show relatively higher values compared to other clusters, suggesting localized repair dynamics possibly related to secondary infrastructure and land-use characteristics.

Cluster 4 (16.89%) represents differentiated recovery concentrated in lower-economic but compact urban areas. This cluster shows a strong negative association with GDP (β=-0.5042) and a positive association with settlement density (β=0.2428), indicating that densely built yet economically weaker neighborhoods formed a distinct recovery regime.

Cluster 5 (20.32%) corresponds to delayed recovery influenced by both environmental and structural factors. Elevation (β=-0.1526) and distance to river (β=-0.1916) exhibit negative associations, while settlement density is also negative (β=-0.2183), suggesting that peripheral or spatially dispersed zones closer to river systems experienced comparatively slower rebound.

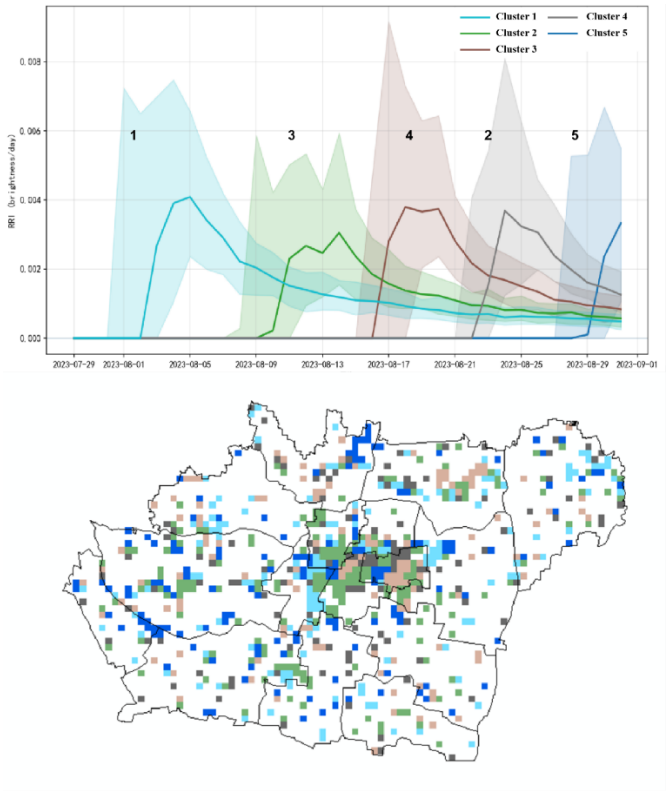

Figure 4. Median recovery trajectories and spatial distribution of the five recovery clusters in Zhuozhou City

Spatially, recovery activity appears distributed across the urban core and surrounding plains rather than concentrated along sharply defined topographic corridors. Unlike mountainous environments, no clear terrain-driven discontinuities are evident, and recovery signals are spatially continuous across much of the built-up area. Correlation analysis further indicates weak monotonic relationships between recovery indicators and individual explanatory variables (Figure 5). For mean recovery rate, all Spearman coefficients remain below 0.04 in absolute value, including GDP density (ρ = 0.02416), elevation (ρ = 0.03676), and settlement density (ρ = -0.04269). Maximum recovery intensity shows similarly weak associations, with the largest Spearman coefficient observed for GDP density (ρ = 0.051998). Recovery onset time exhibits only minor relationships, with elevation presenting the highest absolute value at ρ = -0.07715. These results suggest that recovery heterogeneity in Zhuozhou is not governed by strong single-factor monotonic effects.

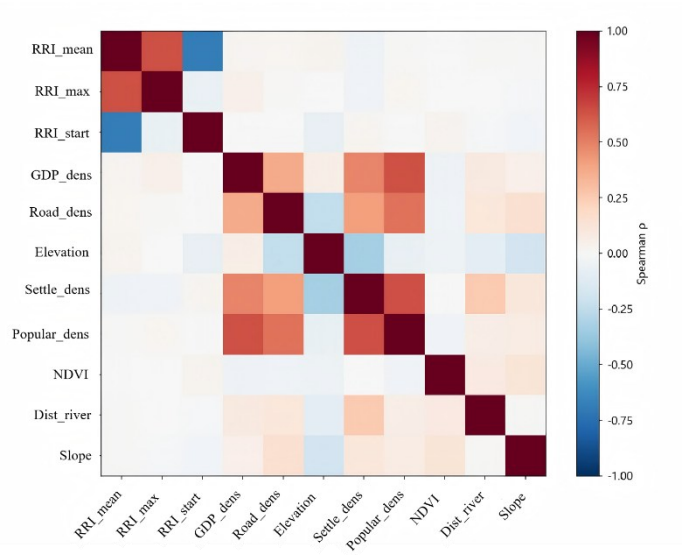

Figure 5. Spearman correlation analysis in Zhuozhou City

Kruskal–Wallis tests confirm statistically significant groupwise differences across recovery clusters for several structural variables. Distance to river ($H = 19.9448$, $p = 0.000512$, $\varepsilon^2 = 0.02106$), GDP ($H = 19.9185$, $p = 0.000518$, $\varepsilon^2 = 0.02103$), and settlement density ($H = 19.0433$, $p = 0.000771$, $\varepsilon^2 = 0.01987$) exhibit the strongest divergence among clusters. Elevation ($H = 11.4012$, $p = 0.02241$) and population density ($H = 10.8599$, $p = 0.02818$) are also significant, though effect sizes remain modest across all variables. Road density, NDVI, and slope do not show statistically significant group differentiation.

Multinomial logistic regression reveals that recovery differentiation emerges primarily through multivariate socioeconomic interactions. GDP exhibits the largest coefficient magnitude across clusters, particularly for Cluster 4 ($\beta = -0.5042$), highlighting the central role of economic capacity in shaping recovery regimes. Settlement density ($\beta = 0.2428$ for Cluster 4; $\beta = -0.2183$ for Cluster 5) further differentiates compact urban areas from peripheral zones. Elevation and river proximity contribute secondary but meaningful variation, especially for Clusters 1 and 5. In contrast, road density, NDVI, and slope display comparatively small coefficients across models.

Taken together, the Zhuozhou case demonstrates that post-rainstorm recovery in a relatively flat urban environment is characterized by structurally balanced recovery modes and weak single-factor dominance. Recovery differentiation is primarily shaped by economic capacity and built-up intensity, while topographic constraints play a comparatively limited role. Unlike terrain-fragmented suburban districts, recovery in Zhuozhou reflects the interplay of urban structural characteristics rather than strong accessibility barriers imposed by elevation or slope.

DISCUSSION

Divergent Recovery Regimes Across Terrain Contexts

The comparative analysis reveals that post-rainstorm recovery dynamics are strongly conditioned by local geomorphological and socioeconomic contexts. Although both Mentougou and Zhuozhou exhibit five identifiable recovery trajectories under a consistent clustering framework, the structural configuration and differentiation mechanisms of these trajectories differ substantially.

In Mentougou, recovery patterns display clear spatial polarization. Delayed and very late recovery clusters occupy a considerable proportion of mountainous areas, while early-onset recovery concentrates along valley corridors and major transport networks. Terrain fragmentation, elevation variation, and accessibility constraints collectively shape the temporal sequencing of restoration activities. In this context, socioeconomic intensity facilitates recovery, yet operates within the structural limits imposed by topography. Elevation and slope function as physical barriers that mediate infrastructure reconnection and repair mobilization, resulting in heterogeneous and spatially discontinuous rebound patterns.

By contrast, Zhuozhou presents a comparatively balanced recovery structure with no dominant delayed cluster. Recovery trajectories are more evenly distributed across the urban landscape, and spatial continuity is more pronounced. Single-variable monotonic associations between recovery indicators and explanatory factors remain weak, and although groupwise differences across clusters are statistically significant, effect sizes are modest. Multivariate modeling indicates that economic capacity and built-up intensity play a more central role in differentiating recovery regimes, while terrain-related variables exert comparatively limited influence. These findings suggest that in relatively flat urban environments, recovery heterogeneity emerges primarily from variations in urban structural configuration and resource allocation rather than from strong physical accessibility constraints.

Taken together, the two cases illustrate distinct recovery regimes shaped by different structural conditions (Table 3). In mountainous suburban districts, terrain-mediated constraints amplify spatial polarization and prolong delayed restoration trajectories. In economically integrated plains cities, recovery differentiation reflects the distribution of economic capacity and urban density rather than geomorphological fragmentation.

Table 3. Cross-case comparison of recovery structures and dominant differentiation factors

Case	Recovery structure	Stronger differentiating factors	Interpretation
Mentougou	Spatially polarized, terrain-fragmented	Population density, elevation, slope, road density	Recovery is strongly conditioned by accessibility and topographic constraints
Zhuozhou	More balanced, structurally continuous	GDP density, settlement density, distance to river	Recovery is more strongly differentiated by urban structural and economic conditions

Terrain-Mediated vs Economically-Mediated Recovery Mechanisms

The empirical contrast between the two cases points to two broader mechanisms underlying post-disaster recovery heterogeneity. The first may be characterized as terrain-mediated recovery, in which geomorphological fragmentation structures accessibility, infrastructure vulnerability, and sequencing of repair activities. Under this regime, elevation, slope, and network connectivity strongly influence the timing and spatial concentration of rebound, and socioeconomic intensity accelerates recovery primarily in areas where physical constraints are manageable.

The second mechanism may be described as economically-mediated recovery, in which economic capacity and built-up intensity shape restoration dynamics in the absence of strong terrain barriers. In this regime, recovery patterns are less polarized and more structurally balanced, and differentiation arises through variations in urban density, economic resources, and spatial organization rather than sharp physical discontinuities. Recovery heterogeneity is therefore less about overcoming physical barriers and more about the allocation of resources and prioritization within a connected urban fabric.

These two mechanisms do not represent mutually exclusive categories but rather context-dependent tendencies. The relative weight of terrain constraints versus socioeconomic structure determines how recovery trajectories unfold. Recognizing this distinction is important for interpreting NTL-derived recovery signals, as identical statistical patterns may reflect fundamentally different underlying processes across geographic contexts.

Implications for Resilience Assessment and Disaster Governance

The findings carry implications for resilience assessment and post-disaster governance. First, the weak monotonic associations observed in Zhuozhou demonstrate that single-factor correlation analysis is insufficient to explain recovery heterogeneity in structurally complex urban systems. Multivariate frameworks are necessary to capture the combined effects of economic capacity, settlement intensity, and environmental conditions. Second, resilience assessment frameworks should explicitly account for terrain context. Applying uniform indicators across mountainous and plain cities may obscure critical structural differences in recovery regimes.

From a governance perspective, terrain-constrained districts require targeted strategies to address accessibility bottlenecks and network fragmentation, whereas economically differentiated plains cities may benefit more from policies that prioritize equitable resource distribution and infrastructure redundancy. Disaster recovery planning should therefore be tailored to local geomorphological and socioeconomic configurations rather than relying on generalized assumptions about urban rebound dynamics.

At the same time, the findings also indicate that NTL-based recovery assessment should be interpreted as one empirical lens on post-disaster resilience rather than a complete resilience measure. NTL is particularly effective for tracing visible functional disruption and restoration associated with electricity-dependent activity, built-up area functioning, and nighttime socioeconomic resumption. Its explanatory power is therefore strongest in hazard contexts that produce detectable nighttime functional disturbance, such as floods, earthquakes, storms, and infrastructure outages. For recovery processes that unfold in sectors less directly expressed in nighttime luminosity, including health services, food provision, telecommunications, or social support, future research should integrate NTL with additional data sources such as mobility records, social media, service accessibility indicators, and sector-specific infrastructure data.

Limitations and Future Research

Several limitations should be acknowledged. First, nighttime light data provide only a partial proxy for post-

disaster recovery. In this study, NTL is used to capture visible functional restoration associated with electricity-dependent activity, built-up area functioning, and nighttime socioeconomic resumption. As such, it may underrepresent recovery processes in sectors that are less directly expressed in nighttime luminosity, including health services, food provision, telecommunications, and social support, and it may also miss restoration activity in low-luminosity or sparsely populated areas.

Second, although cloud screening and data quality controls were applied, residual observational gaps may still influence pixel-level trajectory classification. Third, the explanatory analysis relies on a parsimonious set of eight structural variables and does not include potentially important dimensions such as institutional response capacity, emergency resource allocation, critical facility distribution, infrastructure redundancy, or sector-specific service recovery. The present study therefore offers a deliberately simplified and spatially comparable explanatory model rather than a complete conceptual model of community resilience.

Fourth, the analysis is based on pixel-scale statistical associations and does not establish causal relationships between explanatory variables and recovery outcomes. Finally, the comparative framework is derived from two cases within North China, which limits the broader generalizability of the proposed recovery regimes.

Future research could expand this comparative typology across additional hazard contexts and urban forms, incorporate higher-resolution remote sensing products, and integrate NTL with other data sources such as mobility, communication, public service, or health-related datasets. Such efforts would help develop a more multidimensional and sector-sensitive framework for post-disaster resilience assessment.

CONCLUSION

This study compared post-rainstorm recovery dynamics in two flood-affected areas of North China using daily nighttime light data and structural indicators. Although both cases exhibited five recovery trajectories, their differentiation mechanisms diverged substantially. In mountainous Mentougou, terrain-related constraints structured recovery sequencing and amplified spatial polarization. In contrast, Zhuozhou's relatively flat urban context displayed more balanced recovery patterns, primarily shaped by economic capacity and built-up intensity rather than geomorphological fragmentation.

The comparison suggests that post-disaster recovery is context-dependent and mediated by the interaction between physical terrain and socioeconomic organization. By combining high-frequency nighttime light data, trajectory clustering, and case-specific explanatory modeling, this study provides a transferable empirical framework for identifying visible recovery heterogeneity across urban forms. More broadly, the findings underscore the need for geographically tailored recovery assessment and resilience planning under intensifying climate risks.

ACKNOWLEDGMENTS

This work was supported by the Natural Science Foundation of Beijing (Grant No. L255011, 8242014), the National Natural Science Foundation of China (Grant No. 72521001), the Chinese Academy of Engineering Local Cooperation Project (Grant No. 2025-AHYJY-06), and Strategic Study Project of Chinese Academy of Engineering (Grant No. 2023-JB-08). The authors sincerely acknowledge their support.

REFERENCES

Cutter, S. L. (2016). The landscape of disaster resilience indicators in the USA. Natural Hazards, 80(2), 741-758. https://doi.org/10.1007/s11069-015-1993-2

Intergovernmental Panel on Climate Change. (2023). Climate change 2023: Synthesis report. Contribution of Working Groups I, II and III to the sixth assessment report of the Intergovernmental Panel on Climate Change (Core Writing Team, H. Lee & J. Romero, Eds.). https://www.ipcc.ch/report/sixth-assessment-report-cycle/

Jiang, Y., Yuan, F., Farahmand, H., Acharya, K., Zhang, J., & Mostafavi, A. (2023). Data-driven tracking of the bounce-back path after disasters: Critical milestones of population activity recovery and their spatial inequality. International Journal of Disaster Risk Reduction, 92, 103693. https://doi.org/10.1016/j.ijdrr.2023.103693

Li, X., Zhan, C., Tao, J., & Li, L. (2018). Long-Term Monitoring of the Impacts of Disaster on Human Activity

Using DMSP/OLS Nighttime Light Data: A Case Study of the 2008 Wenchuan, China Earthquake. Remote Sensing, 10(4), 588. https://doi.org/10.3390/rs10040588

Lopes, A. C. R., Rezende, O. M., & Miguez, M. G. (2025). Urban resilience to floods in the context of the disaster risk management cycle: A literature review. Journal of Hydrology, 662, 133827. https://doi.org/10.1016/j.jhydrol.2025.133827

Qiang, Y., Huang, Q., & Xu, J. (2020). Observing community resilience from space: Using nighttime lights to model economic disturbance and recovery pattern in natural disaster. Sustainable Cities and Society, 57, 102115. https://doi.org/10.1016/j.scs.2020.102115

Román, M. O., Wang, Z., Sun, Q., Kalb, V., Miller, S. D., Molthan, A., Schultz, L., Bell, J., Stokes, E. C., Pandey, B., Seto, K. C., Hall, D., Oda, T., Wolfe, R. E., Lin, G., Golpayegani, N., Devadiga, S., Davidson, C., Sarkar, S., ... Masuoka, E. J. (2018). NASA's Black Marble nighttime lights product suite. Remote Sensing of Environment, 210, 113–143. https://doi.org/10.1016/j.rse.2018.03.017

Rose, A., & Dormady, N. (2018). Advances in Analyzing and Measuring Dynamic Economic Resilience. SSRN Electronic Journal. https://doi.org/10.2139/ssrn.3271921

Shu, X., Ye, C., Xu, Z., Liao, R., & Zhang, S. (2025). A multiscale physically-based approach to urban flood risk assessment using ABM and multi-source remote sensing data. International Journal of Disaster Risk Reduction, 119, 105332. https://doi.org/10.1016/j.ijdrr.2025.105332

Tang, L., & Zhang, Y. (2025). Monitoring post-earthquake recovery and conducting impact factor analyses based on nighttime light data. Human Settlements and Sustainability, 1(2), 77-90. https://doi.org/10.1016/j.hssust.2025.04.002

Wang, J., Zhang, J., Gong, L., Li, Q., & Zhou, D. (2018). Indirect seismic economic loss assessment and recovery evaluation using nighttime light images – application for Wenchuan earthquake. Natural Hazards and Earth System Sciences, 18(12), 3253-3266. https://doi.org/10.5194/nhess-18-3253-2018

Yabe, T., Tsubouchi, K., Fujiwara, N., Sekimoto, Y., & Ukkusuri, S. V. (2020). Understanding post-disaster population recovery patterns. Journal of The Royal Society Interface, 17(163), 20190532. https://doi.org/10.1098/rsif.2019.0532

Zhang, D., Huang, H., Roy, N., Roozbahani, M. M., & Frost, J. D. (2023). Black Marble Nighttime Light Data for Disaster Damage Assessment. Remote Sensing, 15(17), 4257. https://doi.org/10.3390/rs15174257

Zheng, J., & Huang, G. (2023). A novel grid cell–based urban flood resilience metric considering water velocity and duration of system performance being impacted. Journal of Hydrology, 617, 128911. https://doi.org/10.1016/j.jhydrol.2022.128911

Zheng, Q., Seto, K. C., Zhou, Y., You, S., & Weng, Q. (2023). Nighttime light remote sensing for urban applications: Progress, challenges, and prospects. ISPRS Journal of Photogrammetry and Remote Sensing, 202, 125-141. https://doi.org/10.1016/j.isprsjprs.2023.05.028